DR. YUXI PANG (Orcid ID : 0000-0001-5039-0236)



Article type : Full Paper

# A unique anisotropic $R_2$ of collagen degeneration (ARCADE) mapping as an efficient alternative to composite relaxation metric ($R_2$-$R_{1\rho}$) in human knee cartilage study

[1]Yuxi Pang, PhD., [2,3]Riann M. Palmieri-Smith, PhD., [1]Dariya I. Malyarenko, PhD., [1]Scott D. Swanson, PhD. and [1]Thomas L. Chenevert, PhD.

[1]Department of Radiology, University of Michigan, Ann Arbor, Michigan, USA; [2]School of Kinesiology and [3]Department of Orthopedic Surgery, University of Michigan, Ann Arbor, Michigan, USA.

**Address correspondence to:**

*Yuxi Pang, PhD*
*Department of Radiology, MRI*
*1500 Central Medical Drive, UH2B205A*
*Ann Arbor, Michigan 48105-0053*
*yuxipang@umich.edu*

**Total words: 4940**

**Purpose:** Anisotropic transverse $R_2$ ($1/T_2$) relaxation of water proton is sensitive to cartilage degenerative changes. The aim is to develop an efficient method to extract this relaxation metric in clinical studies.

**Methods:** Anisotropic $R_2$ can be measured inefficiently by standard $R_2$ mapping after removing an isotropic contribution obtained from $R_{1\rho}$ mapping. In the proposed method, named as a unique ARCADE (Anisotropic $R_2$ of Collagen Degeneration) mapping, an assumed uniform isotropic $R_2$ was estimated at magic angle locations in the deep cartilage, and an anisotropic $R_2$ was thus isolated in a single T2W sagittal image. Five human knees from four volunteers were studied with standard $R_2$ and $R_{1\rho}$ mappings at 3T, and anisotropic $R_2$ derived from ARCADE on one T2W (TE=48.8 ms) image from $R_2$ mapping was compared with the composite relaxation ($R_2 - R_{1\rho}$) using statistical analysis including Student's t-tests and correlations.

**Results:** Anisotropic $R_2$ (1/s) from ARCADE was highly positively correlated with but not significantly different from standard $R_2 - R_{1\rho}$ (1/s) in the segmented deep ($r$=0.83±0.06; 8.3±2.9 vs. 7.3±1.9, $P$ = 0.50) and the superficial ($r$=0.82±0.05; 3.5±2.4 vs. 4.5±1.6, $P$ = 0.39) zones. However, after eliminating systematic errors by the normalization in terms of zonal contrast, anisotropic $R_2$ was significantly higher (60.2±18.5% vs. 38.4±16.6%, $P$ < 0.01) than $R_2 - R_{1\rho}$ as predicted.

**Conclusion:** The proposed anisotropic $R_2$ mapping could be an efficient alternative to the conventional approach, holding great promise in providing both high-resolution morphological and more sensitive imaging from a single T2W scan in a clinical setting.

**Key words:** anisotropic $R_2$; composite relaxation metric $R_2$- $R_{1\rho}$; magic angle effect; chemical exchange effect; human knee cartilage.

## Introduction

Water proton $T_1$ and $T_2$ relaxation times in pure liquids are primarily determined by modulation of the intramolecular dipole-dipole interaction created by molecular isotropic reorientation and characterized by a rotational correlation time $\tau_c$ (1). In biological tissue, magnetization transfer between water and immobilized components affects $T_1$ relaxation times and water exchange between free and restricted domains alters $T_2$ relaxation times. In addition, intricate cellular and microstructural arrangements can restrict molecular reorientation of water creating an orientation-dependent $T_2$ and $T_{1\rho}$ (spin-lattice relaxation time in a rotating frame) in organized tissues such as skeletal muscles and collagen fibers (1-3). A simple method for quick quantification of MR anisotropic relaxation could provide invaluable insights into the integrity of structured tissues.

Articular cartilage (AC) primarily comprises water (~68-85% total weight), structural proteins including mostly collagen (60-80% dry weight) and proteoglycans (~15-40% dry weight), and a sparse distribution (~2%) of chondrocytes (4). Proteoglycans consist of a core with one or more negatively charged linear glycosaminoglycan (GAG) chains covalently attached. In contrast, collagen forms fibrils and fibers intertwined with proteoglycans (4). Histologically, AC could be divided into the superficial (SZ), transitional (TZ) and deep (DZ) zones, where collagen fibers are respectively orientated in parallel, randomly and perpendicularly with respect to the cartilage surface (4-6). These highly organized collagen fibers, particularly in the DZ, create an anisotropic environment for the vast amount of water in cartilage resulting in reported MR relaxation anisotropies (1,7-9).

The orientation-dependent MR relaxation rates $R_1$ $(1/T_1)$, $R_2$ $(1/T_2)$, and $R_{1\rho}$ $(1/T_{1\rho})$ in bovine patellar cartilage-bone specimens have been recently characterized at 9.4T (9). $R_{1\rho}$ was determined with both constant amplitude (CW) and adiabatic waveforms as a function of spin-lock RF power. This study shows that the relaxation rates $R_1$ and $R_2$ had minimal and maximal orientation-dependences, respectively. The orientation anisotropy of $R_{1\rho}$ was almost completely suppressed if a stronger spin-lock RF field was used. More importantly, the relaxation parameters with higher orientation

anisotropies were found to be more sensitive to cartilage degenerative changes secondary to osteoarthritis (OA). In other words, the anisotropic component of $R_2$ (i.e. $R_2^a(\theta)$) has the potential to be a more sensitive MRI biomarker for early cartilage changes in OA and a valuable imaging tool to follow OA progression after anterior cruciate ligament (ACL) reconstruction surgery (10,11).

In conventional $R_2$ mapping, $R_2^a(\theta)$ is not separated from its isotropic counterpart, potentially compromising the sensitivity and specificity of the measure. $R_2$ and $R_{1\rho}$ are currently the most investigated relaxation metrics in clinical studies of knee cartilage degeneration (11-13), but the interpretation of $R_2$ and $R_{1\rho}$ measurements in terms of observed structural protein changes is not straightforward (12,14,15). Most likely, neither $R_2$ nor $R_{1\rho}$ has sufficient sensitivity to the underlying biochemical and physiological changes in cartilage. To increase the sensitivity of MR detection of OA, a composite relaxation metric, $R_2 - R_{1\rho}$, has been proposed (16,17). Subtracting $R_{1\rho}$ from $R_2$ removes the isotropic contribution to $R_2$ to a certain extent if the spin-lock RF used in $R_{1\rho}$ mapping is not strong enough. Previous work has proposed that $R_{1\rho}$ is driven by exchange of hydroxyl protons in GAG with bulk water protons. This hypothesis seems consistent with exchange-driven mechanisms that determine $R_{1\rho}$ (11,17,18) but conflicts with previous findings in cartilage (9,14,15,19-23).

Chemical shift increases linearly with increasing magnetic field ($B_0$) and the relaxation rate $R_2$, due to exchange between protons with different chemical shifts, increases quadratically with $B_0$ (17,18,21). In contrast, the contribution from dipolar interaction to $R_2$ is mostly independent of $B_0$ (21,24). Provided that an increased $R_2$ at a higher $B_0$ could be attributed entirely to the chemical exchange effect, a comparison of $R_2$ at two different $B_0$ should shed light on the relative importance of two different relaxation mechanisms. Mlynarik, et al. performed a detailed study on $R_2$ and $R_{1\rho}$ of human cartilage-bone specimens at 2.95T and 7.05T and concluded that the (residual) dipolar interaction was the dominant relaxation mechanism at $B_0 \leq 3T$ (21).

Later, two clinical studies on healthy human knee cartilage showed that $R_2$ at 7T was either close to (23) or 18% larger than (20) that at 3T, suggesting that the chemical exchange effect would have contributed less than 4% to $R_2$ if it had been measured at 3T.

A similar finding was reported for $R_{1\rho}$ of healthy human knee cartilage, with less than 15% increase at 7T relative to 3T (22). Furthermore, the chemical exchange effect on $R_2$ at 3T can be simulated using published parameters (25), i.e. H2O of 88 [M], GAG of 0.3 [M], exchange rate of 1 kHz and chemical shift of 1 ppm, and it turned out to be a negligible value of 0.05 (1/s) compared with the observed $R_2$ of about 30 (1/s) (20,23).

In this work, we first show theoretically that the $R_2^a(\theta)$ of cartilage at 3T was partially and inefficiently separated in the reported composite relaxation metric (26). The prolonged image acquisition protocol and demanding pulse sequences standardization across different MR systems have prevented the reported method from being favorably accepted by the clinical community (13,17). Hence, an efficient method is proposed here to derive $R_2^a(\theta)$ based on a single T2W sagittal image, by eliminating an assumed constant isotropic $R_2$ contribution derived from the magic angle (MA) locations in the deep cartilage. We refer to our new method as a unique Anisotropic $R_2$ of CollAgen DEgeneration (ARCADE) mapping to emphasize its straightforward association with the integrity of collagen fibers (6,27). The derived femoral cartilage $R_2^a(\theta)$ values in five knees from four volunteers were compared with those of $R_2 - R_{1\rho}$. Our comparable results demonstrate that the proposed ARCADE mapping could be an efficient alternative to the conventional approach, holding great promise in providing both high-resolution morphological and more sensitive $R_2^a(\theta)$ imaging from a single T2W scan in clinical studies on joint cartilage.

**Theory**

For knee cartilage water proton MR relaxation study at 3T, only the intramolecular dipolar interaction between two protons in a water will be considered to interpret the observed MR relaxation rates of $R_1$, $R_2$ and $R_{1\rho}$ (21,24,28). In general, these relaxation rates could be characterized using a two-pool fast exchange model, i.e. water exchange rapidly between the "free" and "bound" pools, and thus represented as the weighted averages of two pools (24) as shown in Eq. 1,

$$R_m = f_i * R_m^i + f_b * R_m^a(\theta) \qquad [1]$$

with m =1, 2 and $1\rho$; $f_i$ and $f_b$ being the molecular fractions of water in the "free" and "bound" pools, with $f_i + f_b = 1$; $R_m^i$ and $R_m^a(\theta)$ being the contributions from a fast

isotropic and a slow anisotropic molecular reorientation (24), which could be characterized respectively by a smaller effective isotropic correlation time ($\tau_f$) and a larger apparent isotropic correlation time ($\tau_b \gg \tau_f$). To simplify the discussion, $R_m^i$ and $R_m^a(\theta)$ can absorb corresponding $f_i$ and $f_b$, to denote the "apparent" relaxation rates in the following unless stated otherwise.

The molecular anisotropic reorientation of the "bound" water in cartilage can be characterized using an axially symmetric model, with a correlation time $\tau_\parallel$ assigned to one rotation about the symmetry axis along the collagen fiber, and another correlation time $\tau_\perp$ to the rotation about an axis perpendicular to the symmetry axis (29). If $\tau_\parallel$ is set to $\tau_f$ and much smaller than $\tau_\perp$ (i.e. $\tau_\perp \gg \tau_\parallel$), corresponding to the "bound" water preferential alignments (1,24,30), the effective correlation time $\tau_b$ of the "bound" water would be determined only by $\tau_\perp$ (29) leading to $\tau_b \gg \tau_f$. This conclusion had been long before stated that the preferential alignments of water molecules could effectively have their otherwise short correlation times amplified by many orders of magnitude (31). Therefore, it would not be surprising to see a significantly larger $\tau_b$ for the restricted water in the "bound" pool.

$R_2^a(\theta)$ can be explicitly written as $R_2^a * (3cos^2\theta - 1)^2/4$, where $R_2^a$ denotes the maximum anisotropic relaxation rate and $\theta$ an angle subtending the dipolar interaction vector and the $B_0$ direction (7,24,32). $R_2^a(\theta)$ reportedly could be effectively suppressed in $R_{1\rho}$ measurements if using a stronger ($\omega_1/2\pi > 2.0$ kHz) spin-lock RF strength (9,19). Accordingly, an effective isotropic correlation time $\tau_b$ for the "bound" water could be estimated to be at least lager than $0.5/\omega_1$. On the other hand, the corresponding $\tau_f$ for the "free" water should be at least larger than $0.62/\omega_0$, given that $R_2 \gg R_1$ (31,33). The Larmor frequency is denoted by $\omega_0/2\pi$ and equal to 128 MHz at 3T.

According to the classical MR relaxation theories (24,34), water proton relaxation rates of $R_1$, $R_2$ and $R_{1\rho}$ could be expressed in terms of an effective isotropic rotational correlation time $\tau_c$ using Eqs. 2-4, and profiled correspondingly at 3T in Fig. 1,

$$R_1 = K\left\{\frac{\tau_c}{1+\omega_0^2\tau_c^2} + \frac{4\tau_c}{1+4\omega_0^2\tau_c^2}\right\} \quad [2]$$

$$R_2 = K\left\{\frac{3\tau_c}{2} + \frac{2.5\tau_c}{1+\omega_0^2\tau_c^2} + \frac{\tau_c}{1+4\omega_0^2\tau_c^2}\right\} \quad [3]$$

$$R_{1\rho} = K\left\{\frac{1.5\tau_c}{1+4\omega_1^2\tau_c^2} + \frac{2.5\tau_c}{1+\omega_0^2\tau_c^2} + \frac{\tau_c}{1+4\omega_0^2\tau_c^2}\right\} \quad [4]$$

where $K$ is a constant of $1.056*10^{10}$ ($s^{-2}$) assuming a distance of 1.59 (Å) between two proton nuclei in water (1,24). If $\tau_c \ll 0.62/\omega_0$ (~$0.8*10^{-9}$ s), all relaxation rates will become $5K\tau_c$, which describes a scenario for water molecules rotating freely in non-viscous liquids (31). In cartilage, however, water can attain a longer $\tau_c$, depending on both interactions with its neighboring macromolecules and their relative orientations to $B_0$ (31).

For the "free" water ($0.62/\omega_0 < \tau_f < 0.5/\omega_1$) in cartilage, $R_{1\rho}^i$ is equal to $R_2^i$, while $R_1^i$ becomes progressively smaller than $R_2^i$ as $\tau_f$ increases. Notably, $R_1^a$ for the "bound" water becomes insignificant, implying that $R_1$ relaxation metric would be orientation-independent and only sensitive to the "free" water (9,32,35,36). For the "bound" water ($\tau_b > 0.5/\omega_1$) in cartilage, $R_{1\rho}^a(\theta)$ is progressively decreased relative to $R_2^a(\theta)$ as $\tau_b$ grows. In this case, $R_{1\rho}^a(\theta)$ can be recast by $R_2^a(\theta)/(1+4\omega_1^2\tau_c^2)$ because of the dominant first term on the right side of Eqs. 3-4. It is worth mentioning that $R_{1\rho}$ will turn into $R_2$ (i.e. $R_2^i$+$R_2^a(\theta)$) and $R_2^i$ respectively when a spin-lock RF is absent and a stronger ($\omega_1\tau_c \gg 0.5$) spin-lock RF is present. Consequently, the reported composite relaxation metric $R_2 - R_{1\rho}$ can be expressed in terms of $R_2^a(\theta)$ as shown in Eq. 5, predicting that $R_2 - R_{1\rho}$ would be a partial $R_2^a(\theta)$ if a spin-lock RF strength is limited in clinical $R_{1\rho}$ mapping (19,37).

$$R_2 - R_{1\rho} = R_2^a(\theta) * \{4\omega_1^2\tau_c^2/(1+4\omega_1^2\tau_c^2)\} \quad [5]$$

Here, we propose an efficient alternative to derive $R_2^a(\theta)$ from one T2W sagittal image, assuming constant proton density ($S_0$) and $R_2^i$ in cartilage (9,32,35). Typically, an orientation-dependent signal intensity $S(\theta)$ in T2W could be written as shown in Eq. 6, including both "free" and "bound" water contributions, with TE being an echo-time (6).

$$S(\theta) = S_0 \exp(-TE * R_2^i - TE * R_2^a(\theta)) \quad [6]$$

$$S(\theta = \pm 54.7°) = S_0 \exp(-TE * R_2^i) \quad [7]$$

$$R_2^a(\theta) = \{\log(S(\theta = \pm 54.7°)) - \log(S(\theta))\}/TE \quad [8]$$

As collagen fibers in the DZ are oriented predominately perpendicular to the cartilage surface (6,32), $R_2^a(\theta)$ will become zero at the magic angles of $\pm 54.7°$ (7,8,32). In this

case, Eq. [6] will reduce to Eq. [7], which represents the "free" water contribution as an internal reference of the assumed constant $S_0 \exp(-TE * R_2^i)$ in the deep cartilage. Combining Eq. 6 and Eq. 7, $R_2^a(\theta)$ could be easily computed using Eq. [8]. This proposed method has leveraged the specific femoral cartilage geometric information that can substitute the otherwise required an additional T2W measurement in conventional $R_2$ mapping.

## Methods

### *Volunteer Subjects*

Four volunteers (V1-V4) were enrolled in this study. The first three had a single knee scanned, while V4 had both knees scanned. Thus, five datasets (S1-S5) were generated and labelled accordingly by the volunteer's sex (M/F), age and knee (L/R) health status (symptomatic [S], asymptomatic [A] or ACL repaired [P]), e.g. V4F20LP in Table 1 and 2. This study was approved by the local institutional review board (IRB) and compliant with the Health Insurance Portability and Accountability Act (HIPAA). Each volunteer was informed about the study and signed a consent form.

### *MR Imaging Protocols*

$R_2$ and $R_{1\rho}$ mappings were performed on a 3T MR scanner using a dedicated 16 Channel T/R Knee Coil. 3D images with different echo times (TE) or spin-lock durations (TSL) were acquired in sagittal plane. An acceleration factor of two was used in fast parallel imaging

*$R_2$ mapping*: An interleaved multi-slice (=43) multi-echo (=8) turbo spin-echo (TSE) pulse sequence was used in image acquisitions with a voxel size of 0.6*0.6*3.0 $mm^3$ and a field of view (FOV) of 128*128*128 $mm^3$ covering entire tibiofemoral compartments (10). The reconstructed images were then interpolated to a voxel size of 0.24*0.24*3.00 $mm^3$. An effective TE for each volumetric image data was n*6.1 ms, with n = 1, 2, 3, 4, 5, 6, 7, 8. TR was 2500 ms, and the total scan time was about 9 minutes per knee.

*$R_{1\rho}$ mapping*: A spin-lock prepared T1-enhanced 3D turbo gradient-echo sequence (T1-TFE) was used to acquire T1$\rho$-weighed images through a segmented elliptic-centric k-space acquisition (38). The spin-lock RF field strength ($\omega_1/2\pi$) was 0.5

kHz, and TSL was 0, 10, 20, 30 and 40 ms, respectively. A similar FOV was used with an acquired voxel size of 0.40*0.40*3.00 $mm^3$ (interpolated to 0.24*0.24*3.00 $mm^3$). The total scan time was about 11 minutes per knee.

***MR Image Post-processing***

All data analysis and image visualization were performed using an in-house software developed in IDL 8.5 (Harris Geospatial Solutions, Inc., Broomfield, CO).

*Image co-registrations:* A free software *Elastix* (39) was used for intra- and inter-series image co-registrations. T2W or T1$\rho$ 3D images with different TE and TSL were first aligned within time-series; then, the aligned T1$\rho$ 3D images were further co-registered to the aligned T2W 3D images. The co-registration scheme was based on a published protocol for human knee cartilage, including a multiresolution approach and a rigid transformation model (40). The co-registration was optimized over 1,000 iterations using a localized mutual information (MI) as a similarity metric, and MI was progressively maximized by minimizing its negative values in the optimization processes. The detailed co-registration parameter settings (par0017) can be found in http://elastix.bigr.nl/wiki.

*Angular-radial segmentation*: First, a whole femoral cartilage was manually delineated using a free software ITK-SNAP (41) for each image slice in T2W and T1$\rho$ 3D data. ROI vertices were placed along cartilage boundaries, with the vertex-path defined as smoothly as possible. Furthermore, non-overlaid cartilage areas (due to motion or misalignment) in both T2W and T1$\rho$ images were minimized in delineating cartilage ROI. Second, the localized cartilage partitions were accomplished by an angular and radial segmentation method (42). Specifically, the vertices (x and y coordinates) from a pre-defined cartilage ROI were used to fit (by a nonlinear least-squares fitting) a virtual circle in each image slice, with the circle center located in femoral condyle (42). Relative to a vertical line, an angle $\varphi$ of a "spoke" connecting each vertex and the circle center could be calculated; subsequently, the whole cartilage was subdivided angularly into 5$^\circ$ partitions based on the range of calculated "spoke" angles. A reference angle (0$^\circ$) was chosen as the $B_0$ direction in a sagittal image, with negative angles pointing to the anterior direction and the positive angles to the posterior direction as shown in Fig. 2. Third, as the shape of femoral cartilage deviates from an ideal half circle, especially on

the lateral sides (43), a segmented angle $\varphi$ had to be re-computed using only adjacent ($\varphi \pm 10°$) vertices to generate a new angle $\theta$ to closely represent collagen fiber orientation in the deep cartilage. Finally, the femoral cartilage was further subdivided radially into the DZ and SZ, with a shared border line having an equidistant to opposite boundaries. This segmented SZ covers at least both the histologically defined the SZ and TZ (4,5).

*$R_2$-$R_{1\rho}$ parametric map:* Both $R_2$ and $R_{1\rho}$ parametric maps were fitted pixel-by-pixel from co-registered multiple 3D data based on a simple exponential relaxation decay model, i.e. $S(t_i) = S_0 \exp(-t_i * P)$, where $P = R_2$ or $R_{1\rho}$, and $t_i$ = [6.1, 12.2, 18.3, 24.4, 30.5, 36.6, 42.7, 48.8] or [0, 10, 20, 30, 40] (ms), respectively. The corresponding parametric error maps were also created by adjusting fitted parameter uncertainties so that the reduced $\chi^2$ was equal to one (44).

*$R_2^a(\theta)$ parametric map from ARCADE:* A single T2W (TE=48.8 ms) 3D dataset from $R_2$ mapping was used. An internal reference corresponding to the "free" water contribution for each image slice was estimated using Eq. 6. Specifically, the average T2W pixel values (in logarithmic scale) within each of segmented ROIs in the DZ were fitted to a function of collagen fiber orientations ($\theta$) as shown in Eq. 9, with parametric bound constraints.

$$y = A - B * (3cos^2(\theta + C) - 1)^2 \qquad [9]$$

The model parameter A was not constrained; however, B and C were limited to the ranges of [0, 10] and [-10°, +10°], respectively. The limited freedom introduced for $\theta$ was to account for potential systematic errors in collagen fiber orientations (5,9).

The nonlinear curve-fitting was performed slice by slice (44).The optimal fits were determined using goodness of fits characterized by $\chi^2$ test statistics with a significant level of $P > 0.95$. Finally, the mean of those determined optimal A values was used as a global internal reference, i.e. $\log\big(S(\theta = 54.7°)\big)$ in Eq. [8].

*Statistical analysis*: The differences and associations between two relaxation metrics were respectively quantified using a Student's paired t-test (a two-tail distribution) and a linear correlation coefficient ($r$), where the statistical significance was considered at $P < 0.05$. Scatterplots were used to demonstrate the potential correlation between two parameters; additionally, data ellipses with a 95% confidence level were

included for visual enhancement (45). A normalized relaxation metric, in terms of zonal contrast, was generated as $(DEEP - SUPF)/DEEP * 100\%$, with $DEEP$ and $SUPF$ representing $R_2^a(\theta)$ or $R_2 - R_{1\rho}$ in the DZ and SZ, respectively. All measurements are shown as mean ± SD unless stated otherwise.

**Results**

A half-circle femoral cartilage sketch is shown in Fig. 2 to illustrate an angular-radial segmentation in a sagittal image, with a highlighted ROI (red square) at a magic-angle orientation in the DZ.

Fig. 3 presents two segmentations (Fig. 3a, c) from an exemplary dataset S4, and comparisons between segmented angles $\varphi$ and locally refined angles $\theta$ in one lateral image slice 14 (Fig. 3a-b) and one medial image slice 23 (Fig. 3c-d) from left knee. Significant larger angle differences (11.0±6.7° vs. 4.3±3.4°, $P < 0.001$) were observed in the medial than those in the lateral side for these two image slices. Specifically, $\varphi$ in Fig. 3d was overestimated ($|\varphi| > |\theta|$) and underestimated ($\varphi < \theta$) in the most anterior and posterior directions, respectively.

An internal reference determination for the same dataset in ARCADE mapping is demonstrated in Fig. 4. A whole deep cartilage T2W map (in logarithmic scale) was generated (Fig. 4a) based on segmented ROIs, where the segmented angles $\varphi$ of $\pm 54.7°$ are indicated by two white dashed lines. An optimal (Fig. 4b, $P = 0.998$) fit and a rejected (Fig. 4c, $P = 0.052$) fit based on the refined angle $\theta$ are shown for the image slice 14 (as shown in Fig. 3a) and 23 (as shown in Fig. 3b), with their spatial locations highlighted by a white and a red arrow in T2W map. For this femoral cartilage, the internal reference was determined as 5.757 ± 0.024.

For the image slice 14 as shown in both Fig. 3a and Fig. 5f, the derived pixel maps of $R_2$ (Fig. 5a), $R_{1\rho}$ (Fig. 5b), $R_2 - R_{1\rho}$ (Fig. 5d) and $R_2^a(\theta)$ (Fig. 5e), along with the ROI-based profile comparisons among $R_2$, $R_{1\rho}$, $R_2 - R_{1\rho}$ and $R_2^a(\theta)$ (Fig. 5c) are presented in Fig. 5. The observed orientation anisotropy of $R_{1\rho}$, compared with $R_2$, was significantly suppressed with a spin-lock RF strength ($\omega_1/2\pi$) of 500 Hz (Fig. 5a-c). Noticeably, $R_2^a(\theta)$ was well aligned with the composite relaxation metric features with increased values and less image blurring (Fig. 5c-e). The image acquisition time for

ARCADE mapping in Fig. 5e was significantly shorter than that for the composite relaxation metric as shown in Fig. 5d (i.e. 1.2 vs. 20 minutes). The T2W image shown in Fig. 5f had an echo-time of 48.8 ms.

For the same dataset S4, Fig. 6 presents the whole knee relaxation parametric maps of $R_2$ (Fig. 6a, e), $R_{1\rho}$ (Fig. 6b, f), $R_2 - R_{1\rho}$ (Fig. 6c, g) and $R_2^a(\theta)$ (Fig. 6d, h) for the DZ (Fig. 6a-d) and the SZ (Fig. 6e-h). Qualitatively, all relaxation rates in the DZ were marginally larger than those in the SZ as previously reported, and $R_2^a(\theta)$ was comparable to $R_2 - R_{1\rho}$.

Scatterplots of $R_2$ versus $R_{1\rho}$ (Fig. 7a) and $R_2^a(\theta)$ versus $R_2 - R_{1\rho}$ (Fig. 7b) are shown in Fig. 7 for quantitative evaluations, with data ellipses overlaid to enhance visualization of existing linear correlations. On average, $R_2$ (1/s) values and their variations were larger than those of $R_{1\rho}$ (1/s) in both the DZ (22.7±8.5 vs. 13.5±2.7) and the SZ (18.5±5.4 vs. 12.6±2.3). In contrast, $R_2^a(\theta)$ (1/s) values and their variances were only marginally larger than those of $R_2 - R_{1\rho}$ (1/s) (i.e. 11.5±9.0 vs. 9.2±7.4 and 6.3±5.9 vs. 5.8±4.9) in these two zones. Unlike the weak associations between $R_2$ and $R_{1\rho}$ ($r$ = 0.54, 0.44, $P$ < 0.01, 0.01), $R_2^a(\theta)$ was highly positively correlated with $R_2 - R_{1\rho}$ ($r$ = 0.91, 0.84, $P$ < 0.01, 0.01) in both segmented cartilage zones.

The average relaxation rates and linear correlation coefficients from each cartilage in the DZ and the SZ are listed in Table 1 and 2 for five examined knees. These tabulated values from the DZ are plotted against those in the SZ as shown in Fig. 8a. The grand means of the average relaxation rates for five knees are represented by each data ellipse centroid. In general, $R_2$ (1/s) was significantly larger than $R_{1\rho}$ (1/s) in the DZ (22.4±2.0 vs. 15.2±1.1, $P$ < 0.01) and the SZ (18.9±2.0 vs. 14.4±1.1, $P$ < 0.01). $R_2^a(\theta)$ (1/s) was hardly distinguishable from $R_2 - R_{1\rho}$ (1/s) in the DZ (8.3±2.9 vs. 7.3±1.9, $P$ = 0.50) and the SZ (3.5±2.4 vs. 4.5±1.6, $P$ = 0.39). However, the normalized $R_2^a(\theta)$, in terms of the zonal difference in cartilage, was significantly larger than the normalized $R_2 - R_{1\rho}$ (i.e. 60.2±18.5% vs. 38.4±16.6%, $P$ < 0.01) as shown in Fig. 8b.

**Discussion**

In this work, we first established that the composite relaxation metric ($R_2 - R_{1\rho}$) actually measures inefficiently a partial anisotropic $R_2$ ($R_2^a(\theta)$) in clinical knee cartilage studies at 3T, and then introduced a new method to extract an uncompromised $R_2^a(\theta)$ based on a single T2W sagittal image. The comparable results between the derived $R_2^a(\theta)$ and the measured $R_2 - R_{1\rho}$ on five femoral cartilages demonstrated that the developed method could be an efficient alternative to the conventional approach.

A key assumption in the new method is a uniform proton density $S_0$ and a constant isotropic $R_2$ ($R_2^i$) regardless its locations and health status in articular cartilage, where the differences in observed $R_2$ relaxation rates stem solely from the "bound" water on differently orientated collagen fibers. This oversimplified view on the "free" water was mainly based on previous observations in that the estimated water content and the observed $R_2$ values at the MA orientations were all nearly uniform across different zones in cartilage (5,9,35,36,46).

For example, one *ex vivo* study showed that $S_0$ was marginally larger in the SZ than in the DZ (i.e. 90 ± 3% vs. 88 ± 4%) at a location near the MA (46). Xia reported an approximately constant $T_2$ (59 ± 6 ms) in cartilage specimens when orientated at the MA in a high-resolution μMRI study (5). He also found that $T_1$ was orientation-independent and almost constant (1.72 ± 0.11 sec), which was confirmed recently by Hänninen, et al. (9). Based on MR relaxation theories, both isotropic $R_2^i$ and $R_1^i$ have nearly linear relationships albeit opposite with an effective correlation time $\tau_f$ of the "free" water in tissue. Thus, a uniform $R_1$ could be reasonably interpreted as a constant $R_2^i$, as the observed $R_1$ in cartilage is dominantly contributed from $R_1^i$.

As articular cartilage has a similar biochemical composition and structural network in extracellular matrix, the "free" water contribution to $R_2$ should not substantially fluctuate in different cartilages; in other words, the internal reference derived from the deep femoral cartilage is applicable to the tibial and patellar cartilages as well. Our preliminary data (not shown) indicated that comparable correlations between $R_2^a(\theta)$ and $R_2 - R_{1\rho}$ were found in the femoral, tibial and patellar cartilages, and an average $R_2^a(\theta)$ in the tibial was almost three times larger than those found in the femoral and patella cartilages.

The assumption used in ARCADE is no exception for an OA population. The integrity of collagen fibers could be compromised due to pathology leading to less preferential orientated water, and the amount of released "free" water would be very small compared to an existing large pool of free water. Although the free water contribution to T2W signal should not be altered in OA subjects, the observed $T_2$ at the locations other than the MA orientations could be increased, which could adversely impact optimal curve-fittings in some image slices and thus potentially lead to a biased internal reference. On the other hand, if localized OA happens to be at the MA sites, the internal reference would not be altered unless an insignificant (<4% at 3T) chemical exchange effect associated with GAG loss be taken into account.

Had the assumption been violated, the derived $R_2^a(\theta)$ would have been offset systematically from its true value as the $R_2^a(\theta)$ computation was just a simple subtraction in logarithmic scale. In this work, the measured $R_2 - R_{1\rho}$ was expected to be smaller than $R_2^a(\theta)$ due to a limited spin-lock RF strength used in $R_{1\rho}$ mapping. According to previous reports (9,19), a spin-lock RF strength of 2.0 kHz could adequately (let's say 99%) suppress $R_2^a(\theta)$, leading to $R_2 - R_{1\rho}$= 99%*$R_2^a(\theta)$. In clinical $R_{1\rho}$ studies at 3T, however, the spin-lock RF strength is usually limited to 0.5 kHz (37), which would translate into $R_2 - R_{1\rho} \approx$ 86%*$R_2^a(\theta)$. On the other hand, the observed $R_2 - R_{1\rho}$ could be erroneously increased due to different data acquisitions (12,13,47), where $R_2$ derived from a multi-echo pulse sequence tends to be more overestimated than $R_{1\rho}$ from a pulse sequence similar to 3D-MAPSS (47). Consequently, the enhanced $R_2 - R_{1\rho}$ could compensate for the loss due to a limited spin-lock RF power, which might justify the comparable $R_2^a(\theta)$ and $R_2 - R_{1\rho}$ observed for some subjects in current study.

Our derived $R_2^a(\theta)$ values generally agreed with the prediction in the DZ except for the first knee (S1). It was quite likely that the determined internal references for S1 in the DZ and for others in the SZ were underestimated leading to an unexpected smaller $R_2^a(\theta)$. However, when using a normalized relaxation metric in terms of zonal contrast such as shown in Fig. 8b, all systematic errors associated with the internal reference and pulse sequences became irrelevant, and the derived normalized $R_2^a(\theta)$ from ARCADE was significantly larger than the normalized $R_2 - R_{1\rho}$ as predicted. Furthermore, the

observed variations in both $R_2^a(\theta)$ and $R_2 - R_{1\rho}$ (Table 1 and 2, Figure 8a and 8b) might reflect collagen fiber unique arrangements due to each volunteer's different age (20-52 yrs.), sex (M/F) and knee health status (ACL repaired, asymptomatic and symptomatic). Even though their true relaxation rates might be systematically offset, the reported significant correlations should not be impaired.

These encouraging comparable results alone would probably not be sufficient to justify an alternative to an established method. However, the great reduction in scan time required for clinical MR studies and the straightforward image post-processing provide a strong impetus for further validating our new method in a large clinical study. Additionally, the quality of derived relaxation metric map from ARCADE could be much better as can be appreciated in $R_2^a(\theta)$ pixel map (Fig. 5e) with respect to $R_2 - R_{1\rho}$ (Fig. 5d). It was likely that the subject had involuntary motions during lengthy data acquisitions and the blurring images were further degraded during the complex co-registration processes in the conventional approach.

As an internal reference method, the developed ARCADE mapping should alleviate any systematic errors known for both $R_2$ and $R_{1\rho}$ mappings due to different pulse sequence implementations on multiple platforms (12,13), making it easier to standardize $R_2^a(\theta)$ measurement in a multi-center trial and be integrated in clinical studies. This new method is independent of the pulse sequence implementation as long as the image pixel intensities are spin-echo weighted, which is inherently insensitive to $B_0$ inhomogeneity. Advanced knee coil provides an excellent $B_1$ homogeneity, with less than ~5% variations in flip angle reported across the cartilage regions of interest in sagittal plane (35). Therefore, ARCADE could be reasonably considered to be insensitive to both $B_0$ and $B_1$ inhomogeneities. In short, an isotropic high-resolution 3D morphological and more relevant and sensitive $R_2^a(\theta)$ relaxation metric imaging could be foreseen with a single scan in clinical setting (48,49) for both knee and other joints.

There are some limitations in present work. First, only five knees were studied, and thus the reported statistical analysis might be biased. Second, the health status of collagen fibers (such as OA) at the MA locations could not be determined as the related residual dipolar interaction is nullified. However, it is possible to remedy this limitation by running an additional T2W sagittal scan with the knee rotated with a small angle along

left-right axis since the proposed method is efficient. Third, no *in vivo* validation against the "gold standard" of diffusion tensor imaging (DTI) was performed. It has been demonstrated that DTI could provide collagen alignment information in human knee cartilage (50). $R_2^a(\theta)$ is mainly induced by restricted water molecular *rotational* diffusion within collagen fibers and the diffusion anisotropy derived from DTI stems largely from water molecular *translational* diffusion along collagen fibers (30,50). It would be interesting to compare how two different water diffusions can be associated with each other. Finally, the potential of the developed method in detecting the earliest cartilage changes that occur in OA might be diminished if GAG depletion is indeed to occur before disruption of the collagen network.

## Conclusions

We have developed an efficient method to measure the collagen orientation-dependent anisotropic transverse water proton relaxation rates in human knee cartilage. The potential to significantly reduce clinical MR scan times and effectively derive more relevant and sensitive information on collagen integrity of both knee and other joints warrants further evaluations and validations in larger clinical studies.

## Acknowledgements

The authors are grateful to Drs. Yansong Zhao and Hui Wang from Philips Healthcare for supporting in optimizing T1ρ data acquisitions and James O'Connor and Suzan Lowe for helping in collecting images.

## References

1. Berendsen HJC. Nuclear Magnetic Resonance Study of Collagen Hydration. J Chem Phys 1962;36(12):3297-3305.
2. Fung BM. Orientation of Water in Striated Frog Muscle. Science 1975;190(4216):800-802.
3. Henkelman RM, Stanisz GJ, Kim JK, Bronskill MJ. Anisotropy of NMR properties of tissues. Magn Reson Med 1994;32(5):592-601.

4. Sophia Fox AJ, Bedi A, Rodeo SA. The basic science of articular cartilage: structure, composition, and function. Sports Health 2009;1(6):461-468.
5. Xia Y. Relaxation anisotropy in cartilage by NMR microscopy (muMRI) at 14-microm resolution. Magn Reson Med 1998;39(6):941-949.
6. Grunder W. MRI assessment of cartilage ultrastructure. NMR Biomed 2006;19(7):855-876.
7. Peto S, Gillis P. Fiber-to-field angle dependence of proton nuclear magnetic relaxation in collagen. Magn Reson Imaging 1990;8(6):705-712.
8. Erickson SJ, Prost RW, Timins ME. The Magic-Angle Effect - Background Physics and Clinical Relevance. Radiology 1993;188(1):23-25.
9. Hanninen N, Rautiainen J, Rieppo L, Saarakkala S, Nissi MJ. Orientation anisotropy of quantitative MRI relaxation parameters in ordered tissue. Sci Rep 2017;7(1):9606.
10. Palmieri-Smith RM, Wojtys EM, Potter HG. Early Cartilage Changes After Anterior Cruciate Ligament Injury: Evaluation With Imaging and Serum Biomarkers-A Pilot Study. Arthroscopy 2016;32(7):1309-1318.
11. Link TM, Neumann J, Li X. Prestructural Cartilage Assessment Using MRI. Journal of Magnetic Resonance Imaging 2017;45(4):949-965.
12. Roemer FW, Kijowski R, Guermazi A. Editorial: from theory to practice - the challenges of compositional MRI in osteoarthritis research. Osteoarthritis Cartilage 2017;25(12):1923-1925.
13. Link TM, Li X. Establishing compositional MRI of cartilage as a biomarker for clinical practice. Osteoarthritis and Cartilage 2018;https://doi.org/10.1016/j.joca.2018.02.902.
14. van Tiel J, Kotek G, Reijman M, Bos PK, Bron EE, Klein S, Nasserinejad K, van Osch GJ, Verhaar JA, Krestin GP, Weinans H, Oei EH. Is T1rho Mapping an Alternative to Delayed Gadolinium-enhanced MR Imaging of Cartilage in the Assessment of Sulphated Glycosaminoglycan Content in Human Osteoarthritic Knees? An in Vivo Validation Study. Radiology 2016;279(2):523-531.

15. Shao H, Pauli C, Li S, Ma Y, Tadros AS, Kavanaugh A, Chang EY, Tang G, Du J. Magic angle effect plays a major role in both T1rho and T2 relaxation in articular cartilage. Osteoarthritis Cartilage 2017;25(12):2022-2030.
16. Pedoia V, Haefeli J, Morioka K, Teng HL, Nardo L, Souza RB, Ferguson AR, Majumdar S. MRI and biomechanics multidimensional data analysis reveals R2 - R1rho as an early predictor of cartilage lesion progression in knee osteoarthritis. J Magn Reson Imaging 2018;47(1):78-90.
17. Russell C, Pedoia V, Majumdar S, Consortium A-A. Composite metric R2 - R1rho (1/T2 - 1/T1rho ) as a potential MR imaging biomarker associated with changes in pain after ACL reconstruction: A six-month follow-up. J Orthop Res 2017;35(3):718-729.
18. Wang P, Block J, Gore JC. Chemical exchange in knee cartilage assessed by R1rho (1/T1rho) dispersion at 3T. Magn Reson Imaging 2015;33(1):38-42.
19. Akella SV, Regatte RR, Wheaton AJ, Borthakur A, Reddy R. Reduction of residual dipolar interaction in cartilage by spin-lock technique. Magn Reson Med 2004;52(5):1103-1109.
20. Gold GE, Han E, Stainsby J, Wright G, Brittain J, Beaulieu C. Musculoskeletal MRI at 3.0 T: relaxation times and image contrast. AJR Am J Roentgenol 2004;183(2):343-351.
21. Mlynarik V, Szomolanyi P, Toffanin R, Vittur F, Trattnig S. Transverse relaxation mechanisms in articular cartilage. J Magn Reson 2004;169(2):300-307.
22. Singh A, Haris M, Cai K, Kogan F, Hariharan H, Reddy R. High resolution T1rho mapping of in vivo human knee cartilage at 7T. Plos One 2014;9(5):e97486.
23. Wyatt C, Guha A, Venkatachari A, Li XJ, Krug R, Kelley DE, Link T, Majumdar S. Improved differentiation between knees with cartilage lesions and controls using 7T relaxation time mapping. J Orthop Transl 2015;3(4):197-204.
24. Momot KI, Pope JM, Wellard RM. Anisotropy of spin relaxation of water protons in cartilage and tendon. NMR Biomed 2010;23(3):313-324.
25. Singh A, Haris M, Cai K, Kassey VB, Kogan F, Reddy D, Hariharan H, Reddy R. Chemical exchange saturation transfer magnetic resonance imaging of human knee cartilage at 3 T and 7 T. Magn Reson Med 2012;68(2):588-594.

26. Pang Y, Palmieri-Smith RM, Chenevert TL. A composite metric R2-R1ρ measures an incomplete anisotropic R2 of human femoral cartilage at 3T. In: Proceedings of the 26th Annual Meeting of ISMRM, Paris, France, 2018. (abstract 3104).
27. Mononen ME, Tanska P, Isaksson H, Korhonen RK. A Novel Method to Simulate the Progression of Collagen Degeneration of Cartilage in the Knee: Data from the Osteoarthritis Initiative. Sci Rep 2016;6:21415.
28. Eliav U, Navon G. A study of dipolar interactions and dynamic processes of water molecules in tendon by 1H and 2H homonuclear and heteronuclear multiple-quantum-filtered NMR spectroscopy. J Magn Reson 1999;137(2):295-310.
29. Woessner DE, Snowden J, B.S. MAGNETIC RELAXATION UNDER HINDERED ROTATION IN FLUIDS. Advan Mol Relaxation Processes 1972;3:181-197.
30. Tourell MC, Momot KI. Molecular Dynamics of a Hydrated Collagen Peptide: Insights into Rotational Motion and Residence Times of Single-Water Bridges in Collagen. J Phys Chem B 2016;120(49):12432-12443.
31. Woessner DE. Nuclear Magnetic-Relaxation and Structure in Aqueous Heterogenous Systems. Mol Phys 1977;34(4):899-920.
32. Xia Y. Magic-angle effect in magnetic resonance imaging of articular cartilage: a review. Invest Radiol 2000;35(10):602-621.
33. Jordan CD, Saranathan M, Bangerter NK, Hargreaves BA, Gold GE. Musculoskeletal MRI at 3.0 T and 7.0 T: a comparison of relaxation times and image contrast. Eur J Radiol 2013;82(5):734-739.
34. Jones GP. Spin-Lattice Relaxation in the Rotating Frame: Weak-Collision Case. PH YSI CAL REVIEW 1966;148(1):332-335.
35. Wang L, Schweitzer ME, Padua A, Regatte RR. Rapid 3D-T(1) mapping of cartilage with variable flip angle and parallel imaging at 3.0T. J Magn Reson Imaging 2008;27(1):154-161.
36. Berberat JE, Nissi MJ, Jurvelin JS, Nieminen MT. Assessment of interstitial water content of articular cartilage with T1 relaxation. Magn Reson Imaging 2009;27(5):727-732.

37. Wang L, Regatte RR. T(1)rho MRI of human musculoskeletal system. J Magn Reson Imaging 2015;41(3):586-600.
38. Li X, Han ET, Busse RF, Majumdar S. In vivo T(1rho) mapping in cartilage using 3D magnetization-prepared angle-modulated partitioned k-space spoiled gradient echo snapshots (3D MAPSS). Magn Reson Med 2008;59(2):298-307.
39. Klein S, Staring M, Murphy K, Viergever MA, Pluim JPW. elastix: A Toolbox for Intensity-Based Medical Image Registration. Ieee T Med Imaging 2010;29(1):196-205.
40. Bron EE, van Tiel J, Smit H, Poot DH, Niessen WJ, Krestin GP, Weinans H, Oei EH, Kotek G, Klein S. Image registration improves human knee cartilage T1 mapping with delayed gadolinium-enhanced MRI of cartilage (dGEMRIC). Eur Radiol 2013;23(1):246-252.
41. Yushkevich PA, Piven J, Hazlett HC, Smith RG, Ho S, Gee JC, Gerig G. User-guided 3D active contour segmentation of anatomical structures: significantly improved efficiency and reliability. Neuroimage 2006;31(3):1116-1128.
42. Kaneko Y, Nozaki T, Yu H, Chang A, Kaneshiro K, Schwarzkopf R, Hara T, Yoshioka H. Normal T2 map profile of the entire femoral cartilage using an angle/layer-dependent approach. J Magn Reson Imaging 2015;42(6):1507-1516.
43. Monk AP, Choji K, O'Connor JJ, Goodfellow JW, Murray DW. The shape of the distal femur: a geometrical study using MRI. Bone Joint J 2014;96-B(12):1623-1630.
44. Markwardt CB. Non-linear Least-squares Fitting in IDL with MPFIT. Astronomical Data Analysis Software and Systems XVIII ASP Conference Series 2009;411:251.
45. Friendly M, Monette G, Fox J. Elliptical Insights: Understanding Statistical Methods through Elliptical Geometry. Stat Sci 2013;28(1):1-39.
46. Goodwin DW, Wadghiri YZ, Dunn JF. Micro-imaging of articular cartilage: T2, proton density, and the magic angle effect. Acad Radiol 1998;5(11):790-798.
47. Matzat SJ, McWalter EJ, Kogan F, Chen W, Gold GE. T2 Relaxation time quantitation differs between pulse sequences in articular cartilage. J Magn Reson Imaging 2015;42(1):105-113.

48. Heule R, Ganter C, Bieri O. Rapid estimation of cartilage T2 with reduced T1 sensitivity using double echo steady state imaging. Magn Reson Med 2014;71(3):1137-1143.
49. Colotti R, Omoumi P, Bonanno G, Ledoux JB, van Heeswijk RB. Isotropic three-dimensional T2 mapping of knee cartilage: Development and validation. J Magn Reson Imaging 2018;47(2):362-371.
50. Raya JG. Techniques and applications of in vivo diffusion imaging of articular cartilage. Journal of Magnetic Resonance Imaging 2015;41(6):1487-1504.

**Tables**

Table 1. Average relaxation rates (1/s) and linear correlation coefficients (*r*) from five femoral cartilages in the deep zone.

| ID | Subject | $\boldsymbol{R_2}$ | $\boldsymbol{R_{1\rho}}$ | r | $\boldsymbol{R_2 - R_{1\rho}}$ | $\boldsymbol{R_2^a(\theta)}$ | r |
|---|---|---|---|---|---|---|---|
| S1 | *V1M52RA* | *24.2 ±6.8* | *15.6 ±3.3* | *0.39* | *8.6 ±6.3* | *4.7 ±6.7* | *0.83* |
| S2 | *V2M47LS* | *19.9 ±6.8* | *14.7 ±3.7* | *0.16* | *5.2 ±7.2* | *5.9 ±7.7* | *0.86* |
| S3 | *V3F41LA* | *20.8 ±6.7* | *15.6 ±3.1* | *0.25* | *5.3 ±6.6* | *9.2 ±7.9* | *0.75* |
| S4 | *V4F20LP* | *22.7 ±8.5* | *13.5 ±2.7* | *0.54* | *9.2 ±7.4* | *11.5 ±9.0* | *0.91* |
| S5 | *V4F20RA* | *24.6 ±8.9* | *16.5 ±4.1* | *0.32* | *8.1 ±8.5* | *10.1 ±8.2* | *0.79* |

*Note*: Relaxation rate is mean ± standard deviation. *P*-value < 0.001 for all correlation coefficients.

Table 2. Average relaxation rates (1/s) and linear correlation coefficients (r) from five femoral cartilages in the superficial zone.

| ID | Subject | $\boldsymbol{R_2}$ | $\boldsymbol{R_{1\rho}}$ | r | $\boldsymbol{R_2 - R_{1\rho}}$ | $\boldsymbol{R_2^a(\theta)}$ | r |
|---|---|---|---|---|---|---|---|
| S1 | *V1M52RA* | *21.7 ±6.6* | *15.7 ±2.9* | *0.34* | *6.0 ±6.3* | *1.6 ±8.1* | *0.87* |
| S2 | *V2M47LS* | *16.0 ±5.8* | *14.0 ±3.7* | *0.50* | *2.0 ±5.0* | *1.0 ±7.2* | *0.76* |
| S3 | *V3F41LA* | *19.1 ±7.7* | *14.7 ±3.0* | *0.15* | *4.3 ±7.9* | *5.8 ±9.6* | *0.87* |

| | | | | | | | |
|---|---|---|---|---|---|---|---|
| S4 | *V4F20LP* | *18.5 ±5.4* | *12.6 ±2.3* | *0.44* | *5.8 ±4.9* | *6.3 ±5.9* | *0.84* |
| S5 | *V4F20RA* | *19.2 ±6.2* | *14.8 ±3.3* | *0.28* | *4.4 ±6.2* | *3.1 ±7.0* | *0.78* |

*Note*: Relaxation rate is mean ± standard deviation. *P*-value < 0.001 for all correlation coefficients.

**Figure Captions**

Fig. 1. Dependences of water proton dipolar relaxation rates (1/s) on an isotropic rotational correlation time $\tau_c$ (s) at 3T ($\omega_0/2\pi$=128 MHz), with $R_1$and $R_2$ depicted respectively in blue and red solid lines, and $R_{1\rho}$in green with $\omega_1/2\pi$=0.5 kHz (solid line), 2.0 kHz (dashed line). Effective correlation times in cartilage are represented by $\tau_f$ and $\tau_b$ for "free" and "bound" water, respectively.

Fig. 2. A schematic diagram of femoral articular cartilage showing an angular-radial segmentation, anatomical annotations and collagen fiber characteristic orientations. The deep and the superficial zones are divided by a red dash-dot line. A segmented ROI, at a magic angle of -54.7° with an angular width of 5° in the deep zone, is highlighted by a red square. The main magnetic field $B_0$ points downwards.

Fig. 3. Two examples of the angular-radial segmentation on a lateral image slice 14 (a) and a medial image slice 23 (c) from dataset S4, and a comparison between segmented angles ($\varphi$) and locally refined angles ($\theta$) for the image slice 14 (a, b) and the image slice 23 (c, d).

Fig. 4. An estimation of the isotropic relaxation contribution to T2W (in logarithmic scale) signal in the deep zone for dataset S4 (a). Examples of an optimal (b) fit and a rejected (c) fit for the image slice 14 (white arrow) and 23 (red arrow) as shown in T2W map (a), with two white dashed lines indicating the segmented angles $\varphi$ of $\pm$54.7°.

Fig. 5. Relaxation rate (1/s) pixel maps of $R_2$ (a), $R_{1\rho}$ (b), $R_2 - R_{1\rho}$ (d) and $R_2^a(\theta)$ (e) for the image slice 14 (from dataset S4) as shown in (f). Derived from the average value within each of segmented ROIs as depicted in (a), the orientation-dependent profiles of $R_2$ (blue triangle), $R_{1\rho}$ (blue square), $R_2 - R_{1\rho}$ (green diamond) and $R_2^a(\theta)$ (red circle) were compared in (c). The echo-time TE was 48.8 ms for the T2W image shown in (f).

Fig. 6. Whole femoral cartilage ROI-based relaxation rate (1/s) maps of $R_2$ (a, e), $R_{1\rho}$ (b, f), $R_2 - R_{1\rho}$ (c, g) and $R_2^a(\theta)$ (d, h) in the deep (a-d) and the superficial (e-h) zones for dataset S4. The slice number and the segmented angle $\varphi$ increase respectively from left (lateral) to right (medial) and up (anterior) to down (posterior). All figures are in the same color scale with the background set to zero (black).

Fig. 7. Scatterplots of relaxation rates (1/s) of $R_2$ vs. $R_{1\rho}$ (a) and of $R_2^a(\theta)$ vs. $R_2 - R_{1\rho}$ (b) in the deep (red circle) and the superficial (blue cross) zones with each data ellipse superimposed for dataset S4. The linear correlation coefficients ($r$) are included in the plots.

Fig. 8. A scatterplot of the means of relaxation rates (1/s) of $R_2$ (magenta star), $R_{1\rho}$ (green triangle), $R_2 - R_{1\rho}$ (blue diamond) and $R_2^a(\theta)$ (red circle) in the deep zone against those in the superficial zone (a) with subgroup data ellipse superimposed, and a comparison between normalized $R_2^a(\theta)$ (yellow) and normalized $R_2 - R_{1\rho}$ (blue) for five knees (b).

**Tables**

Table 1. Average relaxation rates (1/s) and linear correlation coefficients (r) from five femoral cartilages in the deep zone.

| ID | Subject | $R_2$ | $R_{1\rho}$ | r | $R_2 - R_{1\rho}$ | $R_2^a(\theta)$ | r |
|---|---|---|---|---|---|---|---|
| S1 | V1M52RA | 24.2 ± 6.8 | 15.6 ± 3.3 | 0.39 | 8.6 ± 6.3 | 4.7 ± 6.7 | 0.83 |
| S2 | V2M47LS | 19.9 ± 6.8 | 14.7 ± 3.7 | 0.16 | 5.2 ± 7.2 | 5.9 ± 7.7 | 0.86 |
| S3 | V3F41LA | 20.8 ± 6.7 | 15.6 ± 3.1 | 0.25 | 5.3 ± 6.6 | 9.2 ± 7.9 | 0.75 |
| S4 | V4F20LP | 22.7 ± 8.5 | 13.5 ± 2.7 | 0.54 | 9.2 ± 7.4 | 11.5 ± 9.0 | 0.91 |
| S5 | V4F20RA | 24.6 ± 8.9 | 16.5 ± 4.1 | 0.32 | 8.1 ± 8.5 | 10.1 ± 8.2 | 0.79 |

Note: Relaxation rate is mean ± standard deviation. P-value < 0.001 for all correlation coefficients.

Table 2. Average relaxation rates (1/s) and linear correlation coefficients (r) from five femoral cartilages in the superficial zone.

| ID | Subject | $R_2$ | $R_{1\rho}$ | r | $R_2 - R_{1\rho}$ | $R_2^a(\theta)$ | r |
|---|---|---|---|---|---|---|---|
| S1 | V1M52RA | 21.7 ± 6.6 | 15.7 ± 2.9 | 0.34 | 6.0 ± 6.3 | 1.6 ± 8.1 | 0.87 |
| S2 | V2M47LS | 16.0 ± 5.8 | 14.0 ± 3.7 | 0.50 | 2.0 ± 5.0 | 1.0 ± 7.2 | 0.76 |
| S3 | V3F41LA | 19.1 ± 7.7 | 14.7 ± 3.0 | 0.15 | 4.3 ± 7.9 | 5.8 ± 9.6 | 0.87 |
| S4 | V4F20LP | 18.5 ± 5.4 | 12.6 ± 2.3 | 0.44 | 5.8 ± 4.9 | 6.3 ± 5.9 | 0.84 |
| S5 | V4F20RA | 19.2 ± 6.2 | 14.8 ± 3.3 | 0.28 | 4.4 ± 6.2 | 3.1 ± 7.0 | 0.78 |

Note: Relaxation rate is mean ± standard deviation. P-value < 0.001 for all correlation coefficients.

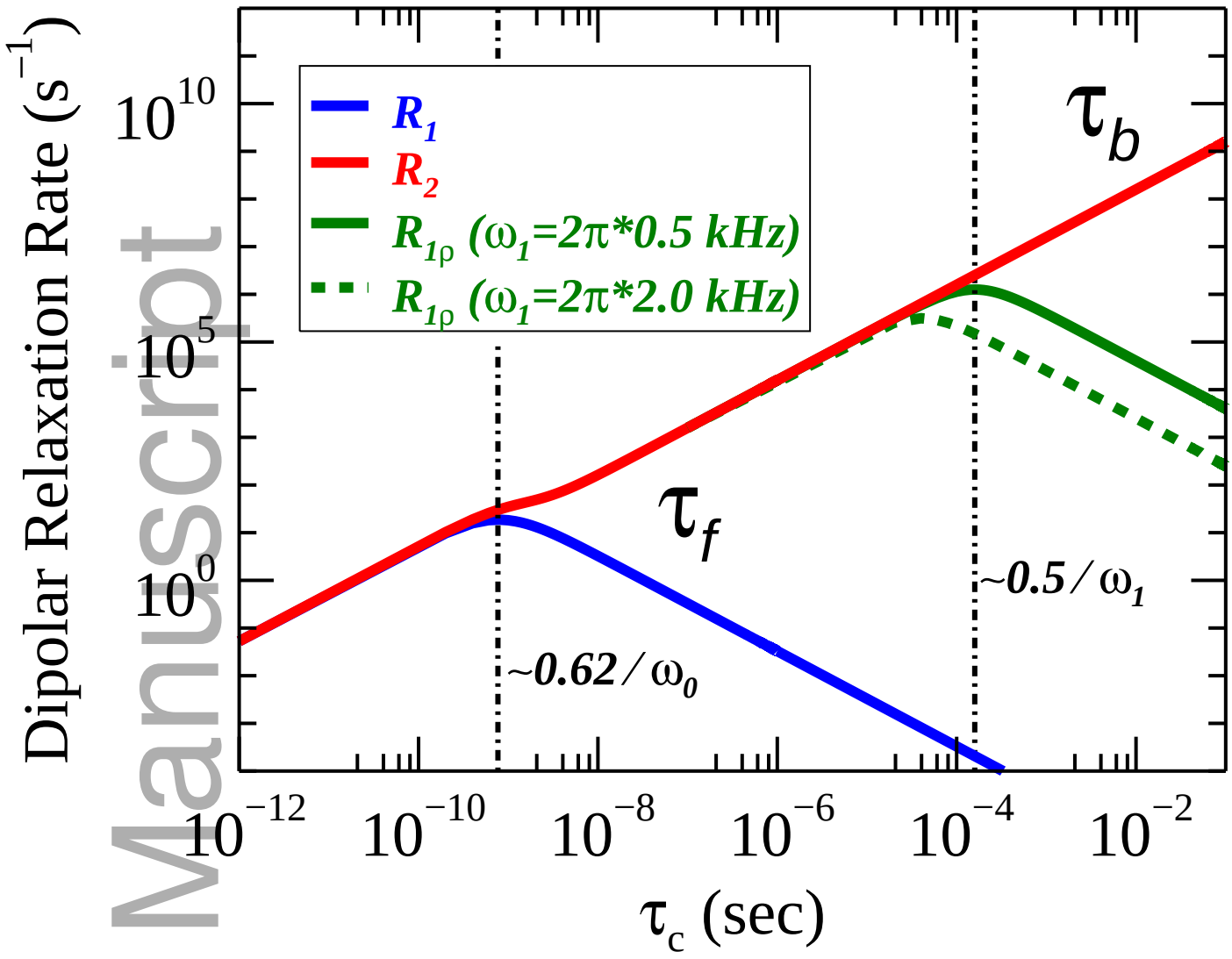


mrm_27621_f1.eps

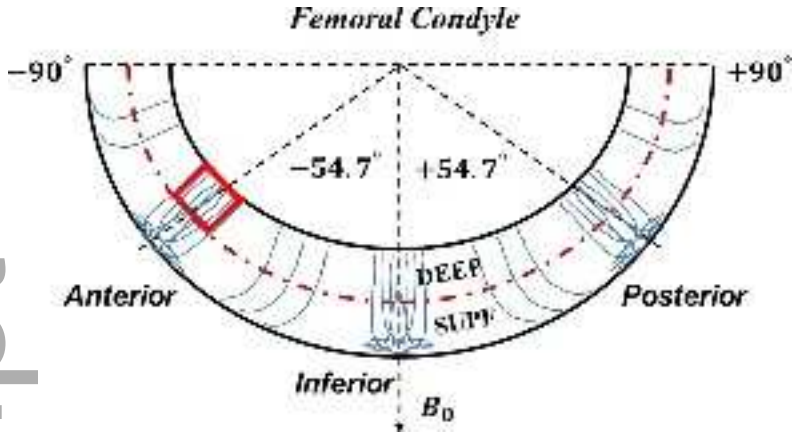


mrm_27621_f2.tif

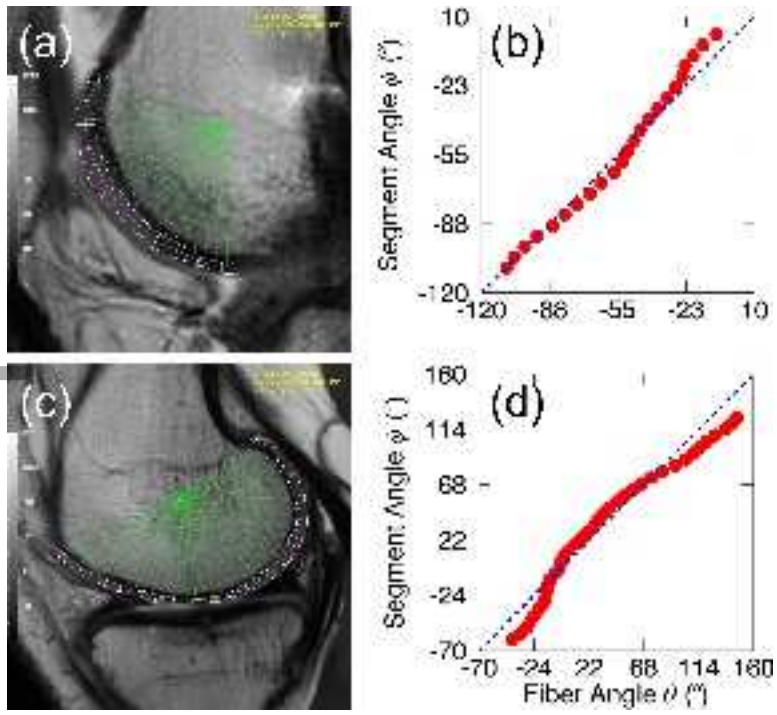


mrm_27621_f3.tif

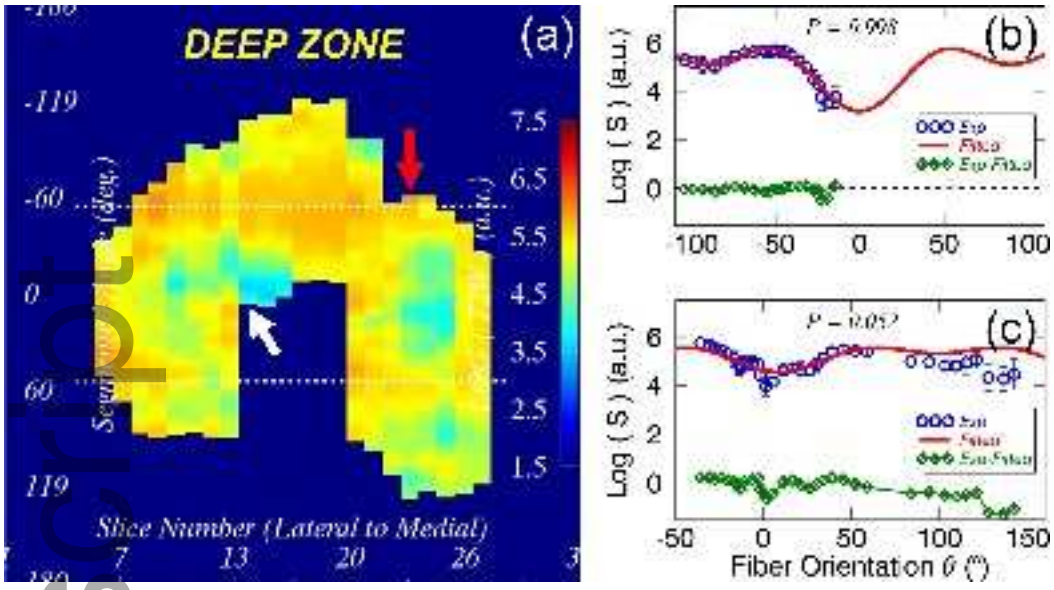


mrm_27621_f4.tif

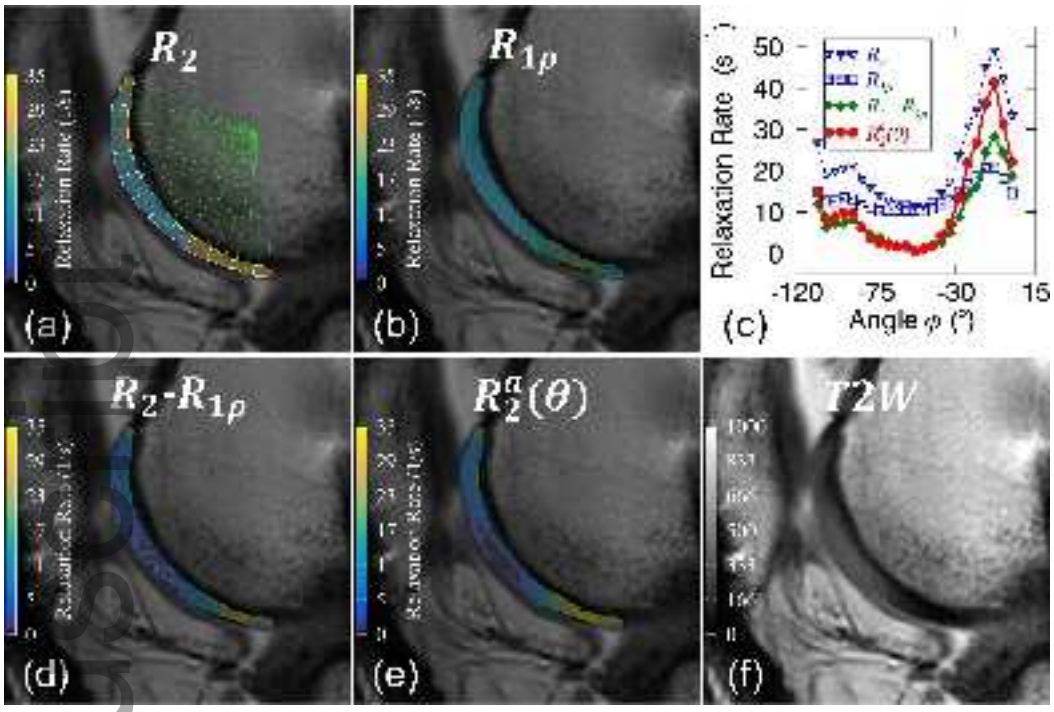


mrm_27621_f5.tif

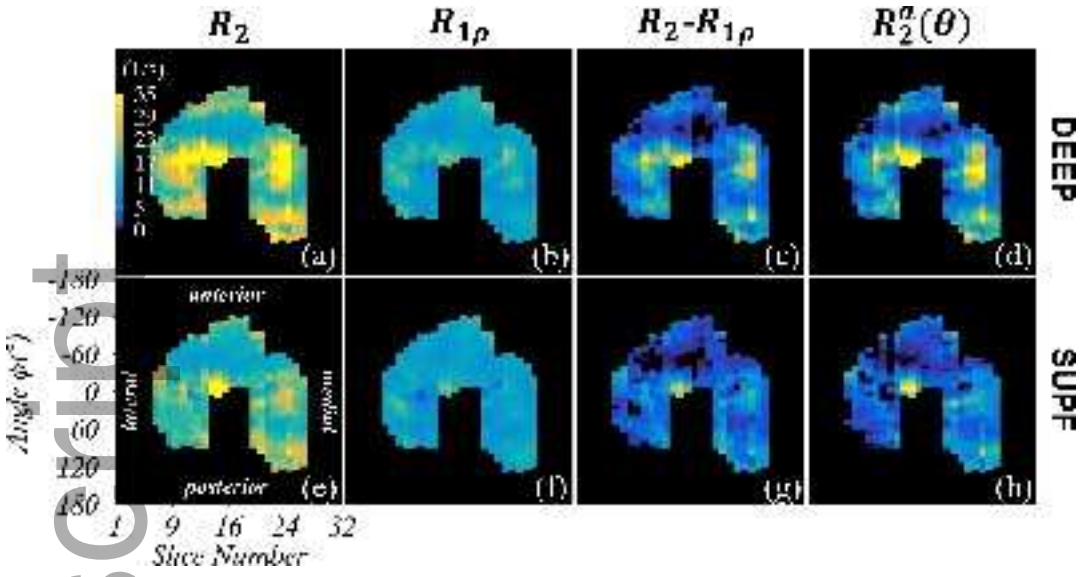


mrm_27621_f6.tif

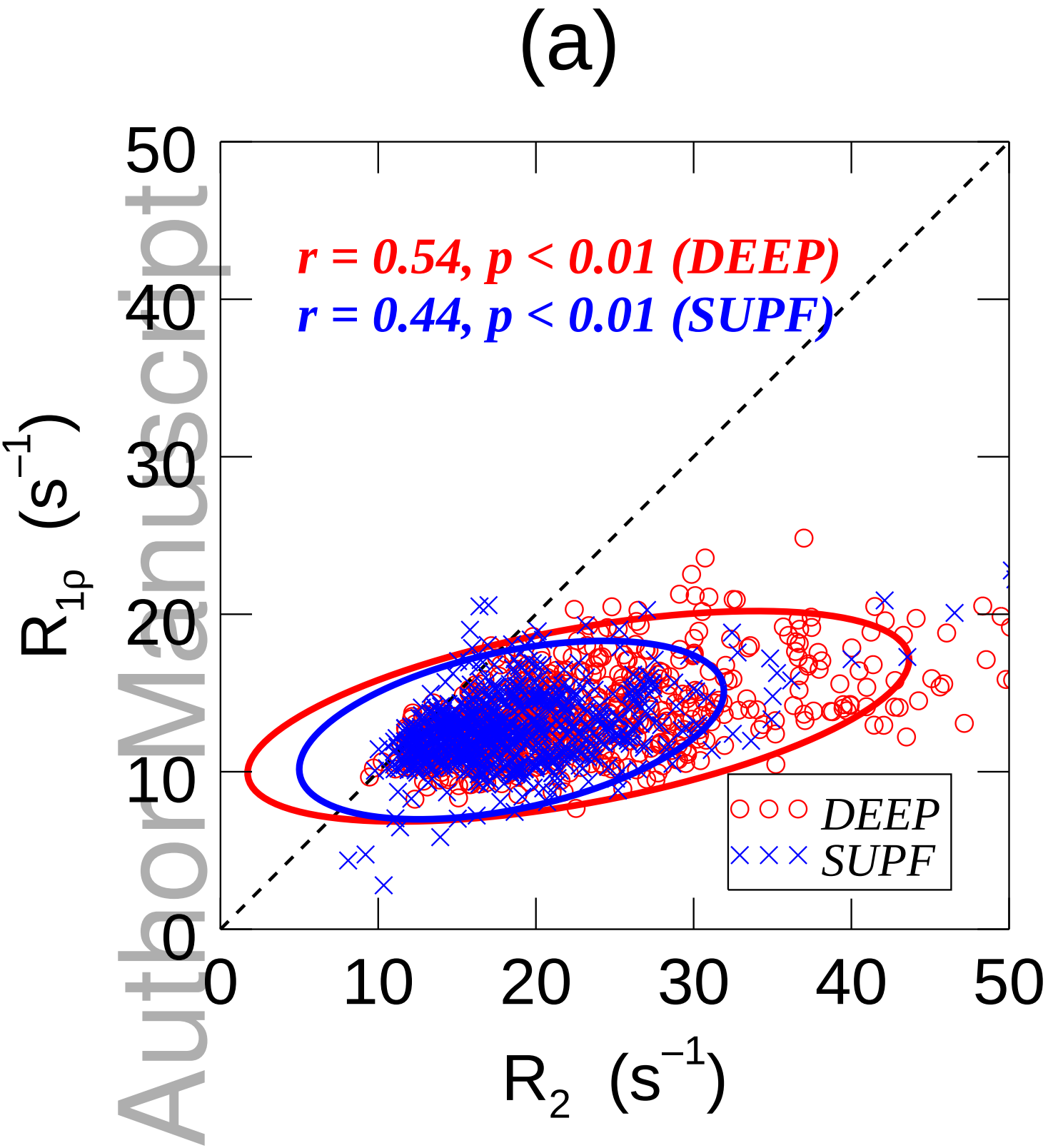


mrm_27621_f7a.eps

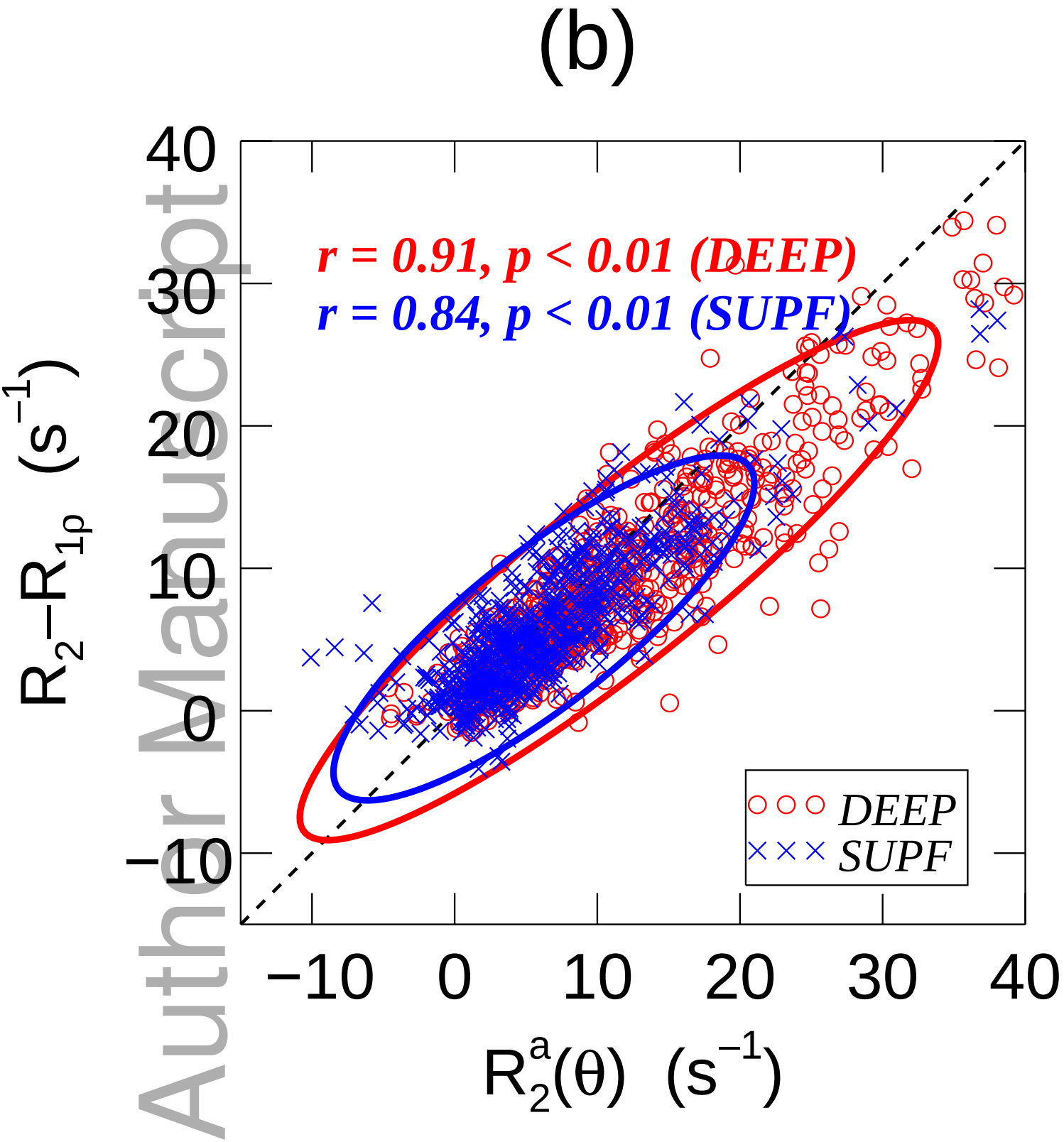


mrm_27621_f7b.eps

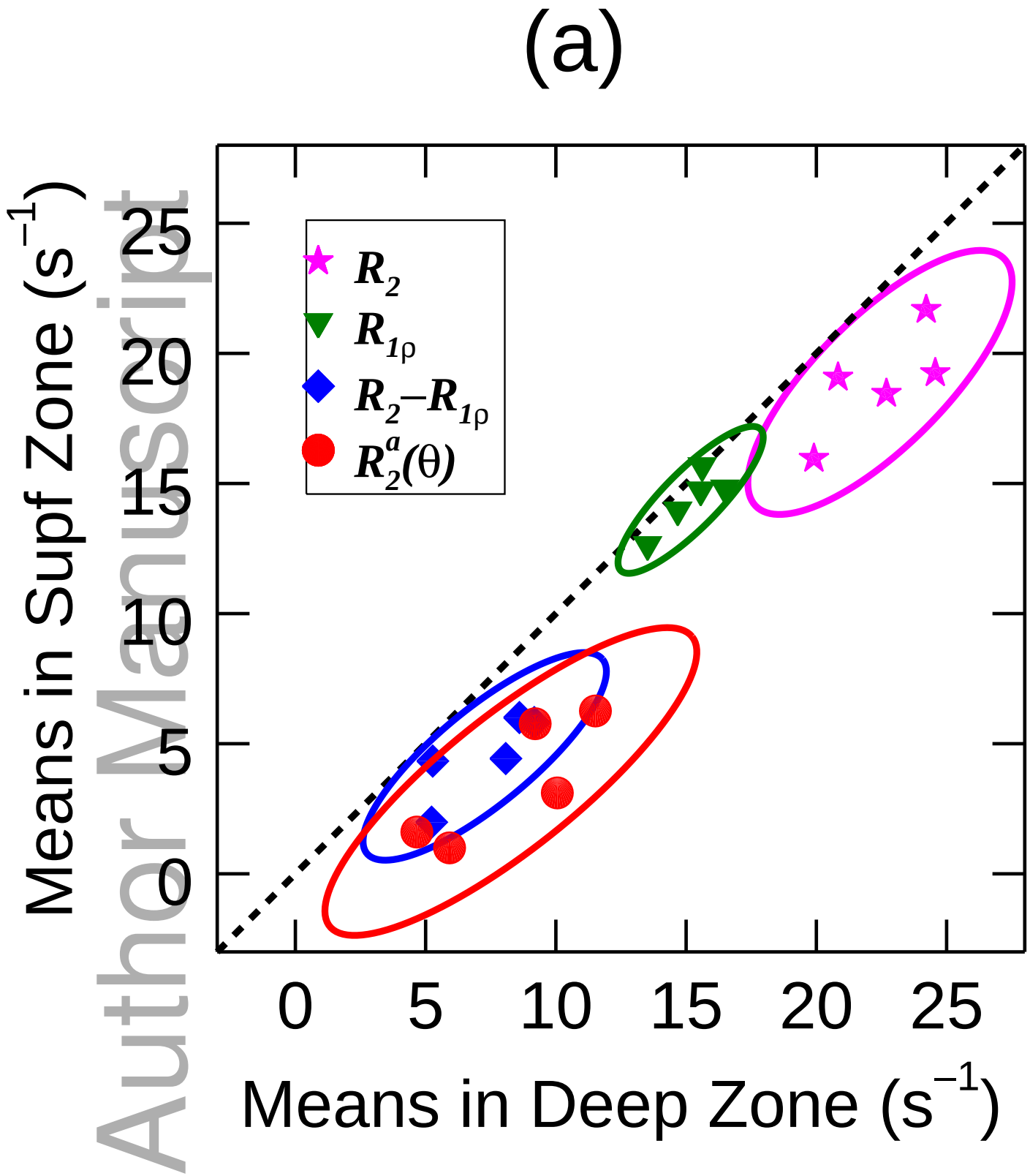


mrm_27621_f8a.eps

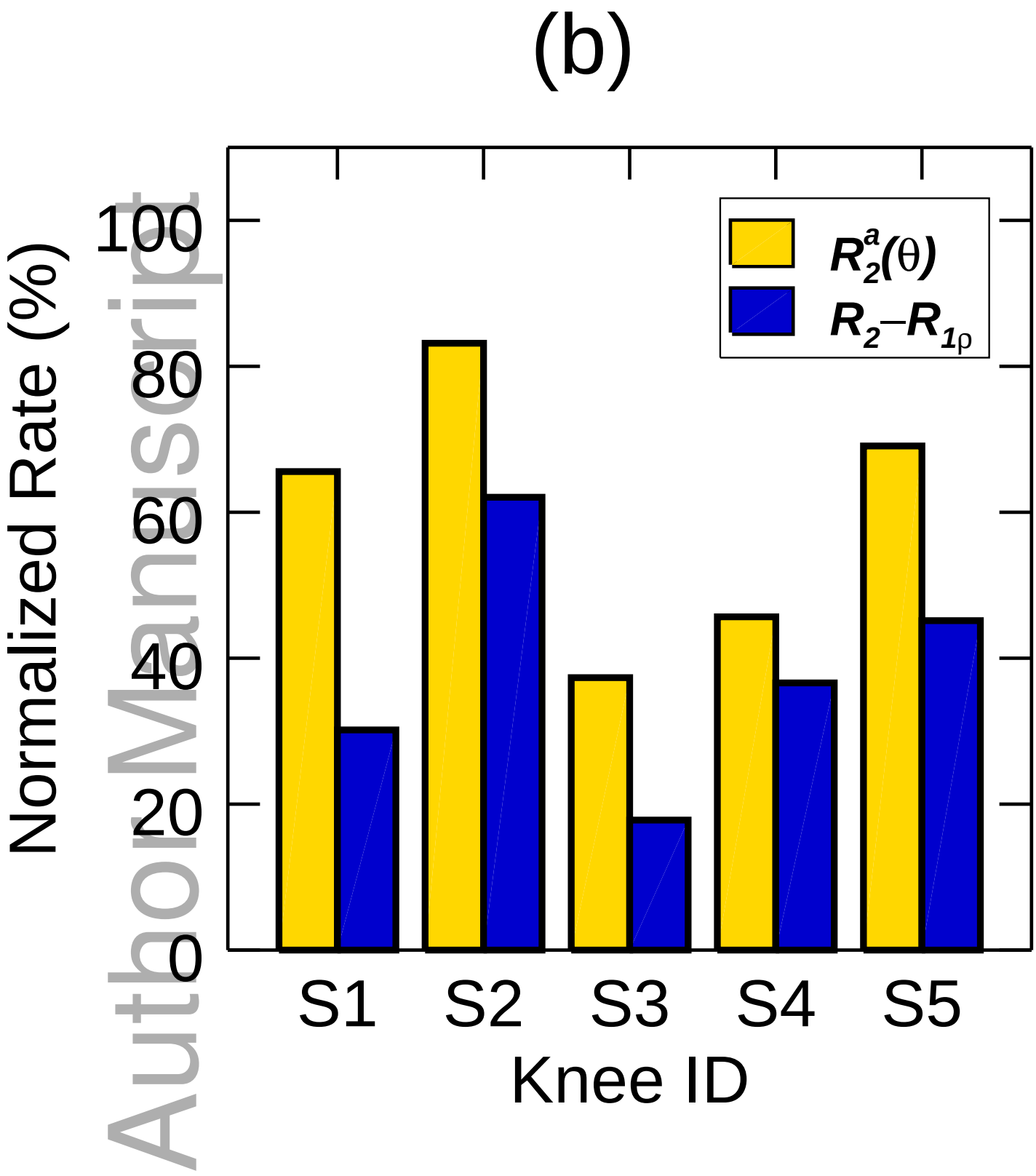




mrm_27621_f8b.eps